Discovery of Early Mesozoic Magmatism in the Northern Muglad Basin (Sudan): Assessment of Its Impacts on Basement Reservoir

Jian Zhao[1,2] and Lirong Dou[1,2]*

[1]Research Institute of Petroleum Exploration and Development, PetroChina, Beijing, China, [2]China National Oil and Gas Exploration and Development Company Ltd., Beijing, China

The crystalline basement in the Central African Rift System (CARS) has been confirmed as a good unconventional reservoir in the surrounding basins of the Muglad area, Sudan. This study has recognized at least five Early Mesozoic intrusions for the first time at the northern margin of the Muglad Basin. Field and petrographic investigations show that they are mainly granite, syenite, diorite, and monzonite, with dominant alkali feldspar, plagioclase, quartz, and minor hornblende, biotite, and magnetite. Zircon internal structures, Th/U ratios, and rare earth element (REE) patterns indicate their magmatic origin. A total of 210 zircons from five samples were analyzed using LA-ICP-MS and they yielded U-Pb ages from 195.0 ± 6 to 225.0 ± 3 Ma, belonging to the Late Triassic-Early Jurassic. These results suggest that the Muglad Basin basement is not universally Precambrian as previously considered. The older basement was intruded and modified by Early Mesozoic magmas as evidenced by field contacts and our dating results. These magmatic events produced diverse Mesozoic igneous rocks prior to the formation of the Muglad Basin (Early Cretaceous), becoming new members of the crystalline basement. This composite basement then experienced prolonged weathering and fracturing for 65–95 Ma, resulting in porous and permeable weathered layers or fractured zones, making the basement a good unconventional reservoir for oil and gas.

Keywords: Zircon U-Pb age, lithological characteristics, Mesozoic intrusions, Precambrian basement, unconventional reservoir, Muglad Basin, Sudan

INTRODUCTION

Basement rocks are key in studying the formation and evolution of rift basins, and their lithological characteristics, generation, and homogeneity also directly affect their exploration potential and economic values, such as the bearing of metals or the development of oil and gas reservoirs. The Central African Rift System (CARS) is an intracontinental Cretaceous–Paleogene rift system with dozens of well-known prolific basins, such as the Bongor, Doba, Doseo, Salamat, Melut, and Muglad basins, where encouraging oil and gas resources have been successively discovered. These trans-extensional or extensional basins were mainly formed during the Early Cretaceous on the Precambrian crystalline basement (Fairhead J. D., 1988; Binks and Fairhead, 1992; Guiraud and Maurin, 1992; Genik, 1993; Fairhead et al., 2013). Regionally, these rift basins have experienced the Precambrian-Late Jurassic pre-rift stage (the craton), the Early Cretaceous- Late Cretaceous rift stage
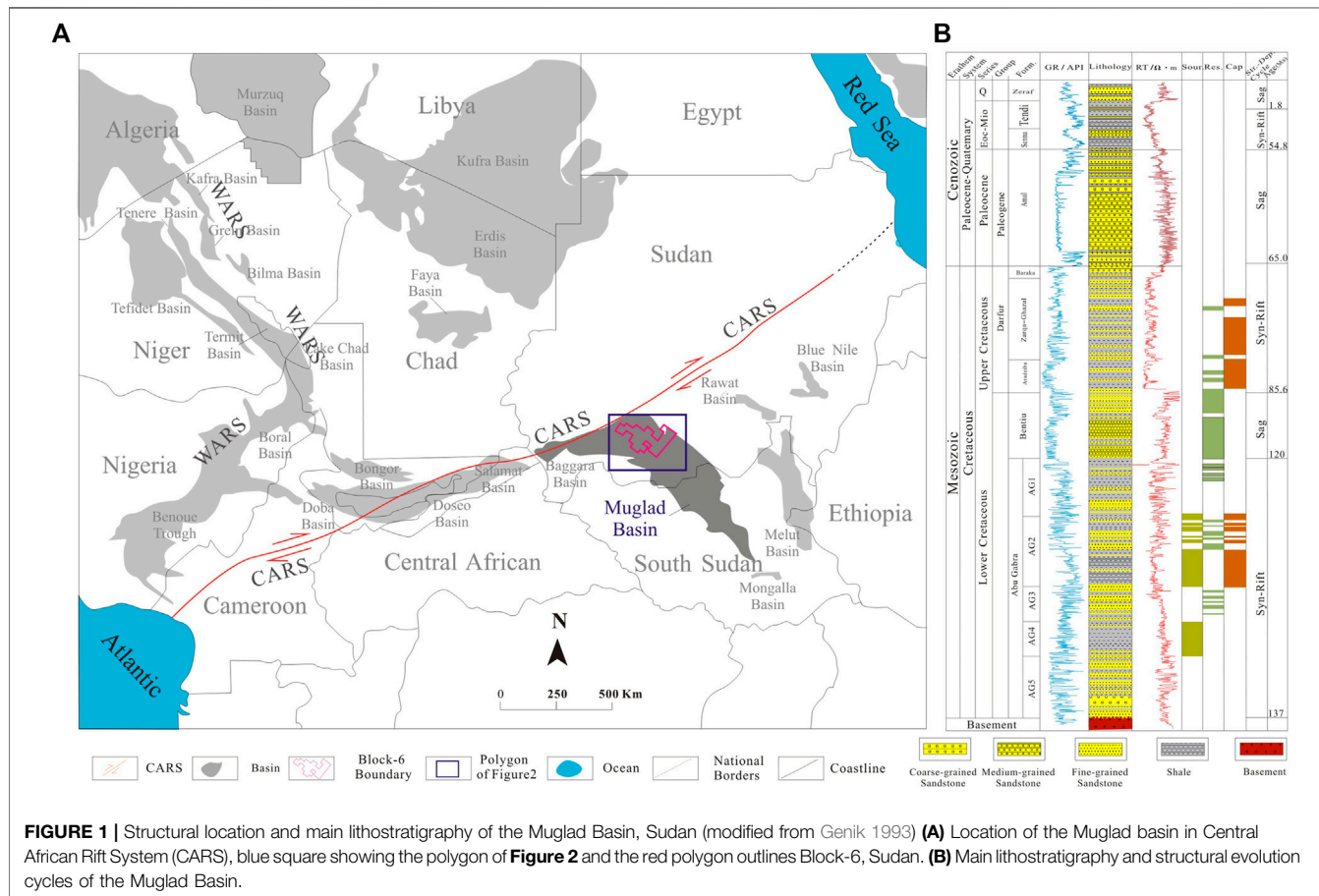
(evolution of fault sags and depressions), and the Paleogene-current post-rift stage (Schull, 1988; Genik, 1992; McHargue et al., 1992; Genik, 1993). The Precambrian-Late Jurassic craton stage has been generally regarded as the main period of the regional basement formation. Although the latter two stages were respectively dominated by intraplate rifting and depression sedimentation, the basement has been mostly inherited and preserved, without significant changes in lithology. As a result, it has been widely accepted that the basements across the Central African Rift System (CARS) should be similar or homogeneous, and comparable among different basins (Fairhead J. D., 1988; Schandelmeier and Pudlo, 1990; Guiraud et al., 1992; Guiraud and Maurin, 1992).

Previously, both regional geological surveys and intensive oil and gas exploration activities in the CARS have proved and even addressed that the basement in the CARS only consists of ancient Precambrian rocks. For example, the basement in southwestern Chad is composed of Precambrian granite, granodiorite, and granitic gneisses (Penaye et al., 2006). Some Precambrian marble was also discovered locally and reported by Penaye et al. (2006), which added a new rock member to the granitic basement. In the neighboring Melut basin in Sudan, the granite, granodiorite, and gneisses in the basement have consistent geological ages of ca. 540 Ma (Schull, 1988; Awad, 2015). Likewise, in the Bongor basin (Chad), at least two major groups of rocks were identified, including magmatic rocks with ages between 621 Ma and 525 Ma and metamorphic rocks between 616 Ma and 526 Ma (Dou et al., 2015; Li et al., 2017; Dou et al., 2018).

In 2018, high oil flows were tested from basement buried hills in the Bongor Basin (Chad), providing a new perspective of basement study that greatly boosted the related research not only for fundamental geology but also for evaluation of unconventional reservoirs. The basement reservoirs in the Bongor Basin are classic buried hills where the reservoir is a combination of the weathered, leached, and fractured basement. The exposure and weathering of the fractured basement provide good conditions for storing and transporting hydrocarbons (Dou et al., 2018). The lithology of the basement has fundamental impacts on the development of the unconventional reservoir. The buried hills' morphology, their burial depth, and their relationship to major faults will also affect the degree of reservoir development (Dou et al., 2015; Li et al., 2017; Dou L. et al., 2018). Besides, time also plays a key role in reservoir development. The longer duration of the basements was weathered and fractured, the better a basement reservoir could be developed.

However, our current understanding of the Muglad Basin, such as the fundamental lithology of the basement, and the potential as an unconventional reservoir, are still very limited compared to other CARS basins. Vail (1972) suggested that the basement of the Muglad Basin was composed of Precambrian

FIGURE 1 | Structural location and main lithostratigraphy of the Muglad Basin, Sudan (modified from Genik 1993) **(A)** Location of the Muglad basin in Central African Rift System (CARS), blue square showing the polygon of **Figure 2** and the red polygon outlines Block-6, Sudan. **(B)** Main lithostratigraphy and structural evolution cycles of the Muglad Basin.
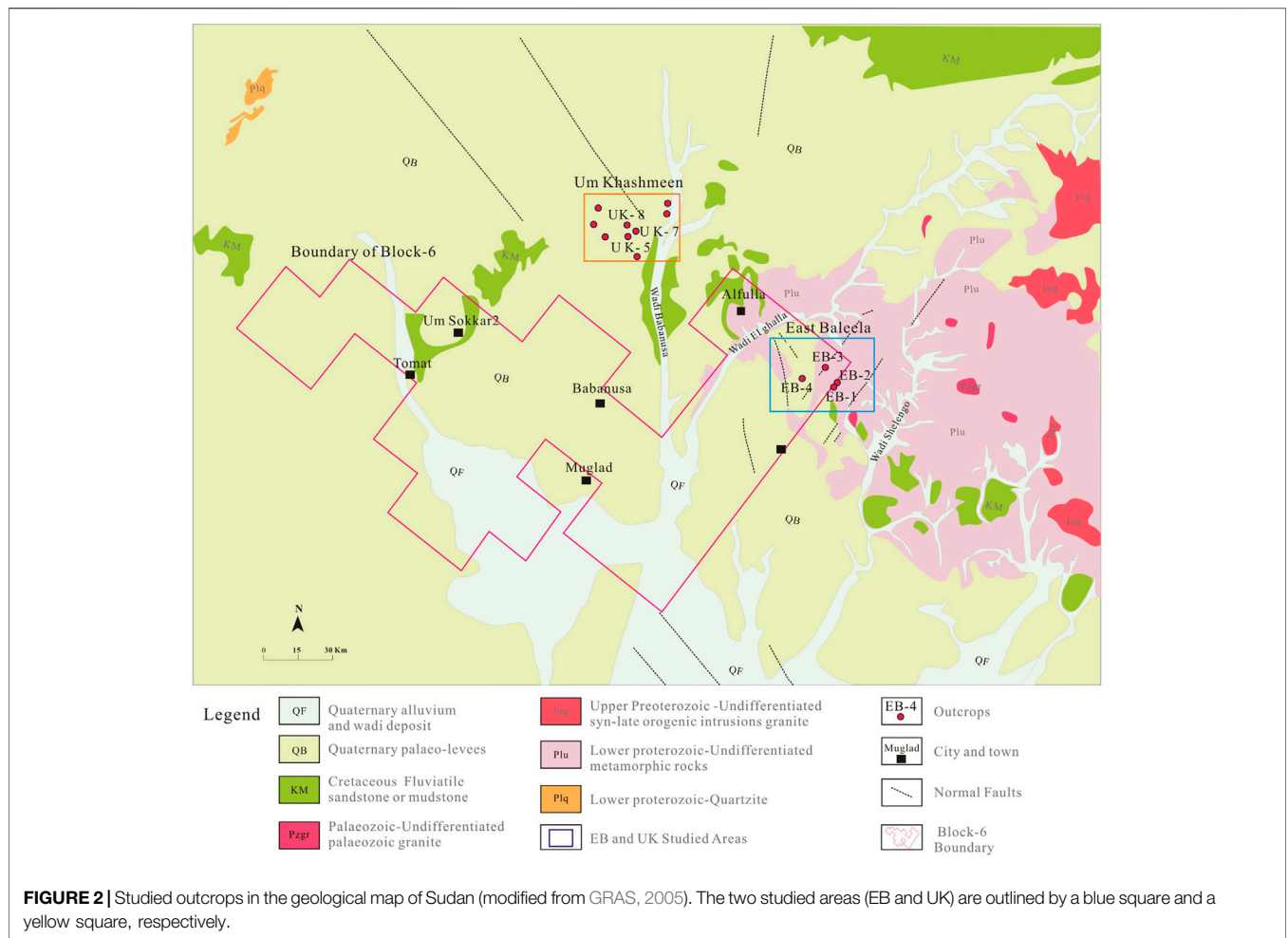
FIGURE 2 | Studied outcrops in the geological map of Sudan (modified from GRAS, 2005). The two studied areas (EB and UK) are outlined by a blue square and a yellow square, respectively.

rocks, including granite, granodiorite, granitic gneiss, and amphibolite, etc, without providing ages of these rocks. Zhao et al. (2020) further documented the dominated granitoids of the Muglad Basin basement underwent variable degrees of regional metamorphism, but no ages were available.

In this study, we conducted a detailed geological survey and collected samples along the north margin of the Muglad basin to study the lithology diversity and chronology of the basement rocks. The results will help to assess whether the basement of the Muglad basin is a potential target for a good unconventional reservoir.

GEOLOGICAL SETTINGS

Muglad Basin lies in the southern part of the Republic of Sudan, crossing Sudan and the Republic of South Sudan. It extends about 800 km long and 200 km wide, covering an area of more than $12 \times 10^4 \, km^2$. This basin is a Cretaceous rift basin developed on the Precambrian crystalline basement (Fairhead J. D., 1988; Fairhead J. D., 1988; Schandelmeier and Pudlo, 1990; Fairhead, 1992; Guiraud et al., 1992; Guiraud and Maurin, 1992; Tong et al., 2004; Yassin et al., 2017), and located on the south part of the

Central African Rift System (CARS). The NW-SE trending basin extends towards the northwest where it terminates at the CARS and gradually converges toward the southeast (Genik, 1992; Genik, 1993) (**Figure 1A**). In terms of the Exploration & Production (E&P) block division, the northern part of the Muglad basin is in Block-6 (outlined in red in **Figure 1A**), which was operated by China National Petroleum Company (CNPC).

Throughout the tectonic evolution of the CARS, three major rifting-sagging cycles have been identified in the Muglad Basin (Fairhead, 1988; Schull, 1988; Genik, 1992; Genik, 1993). 1) Abu Gabra-Bentiu cycle, with strong rifting and faulting movement, the Abu Gabra Formation (Fm.) is the earliest syn-rift sequence and consists of conglomerates at the bottom, sandstone and mudstone, and organic-rich shale in the upper intervals. After that, a thick layer of sandstone was deposited in the Bentiu Fm. as the first sag system. 2) Darfur-Amal cycle, with relatively weaker tectonic movement, the shaly sedimentary sequence was developed in the Darfur Group and was followed by a thicker layer of sandstone in Amal. 3) Eocene-present period, with the weakest rifting stage in the Early Paleogene, is characterized by interbedded sandstone and shale with uneven distribution in different areas (**Figure 1B**).
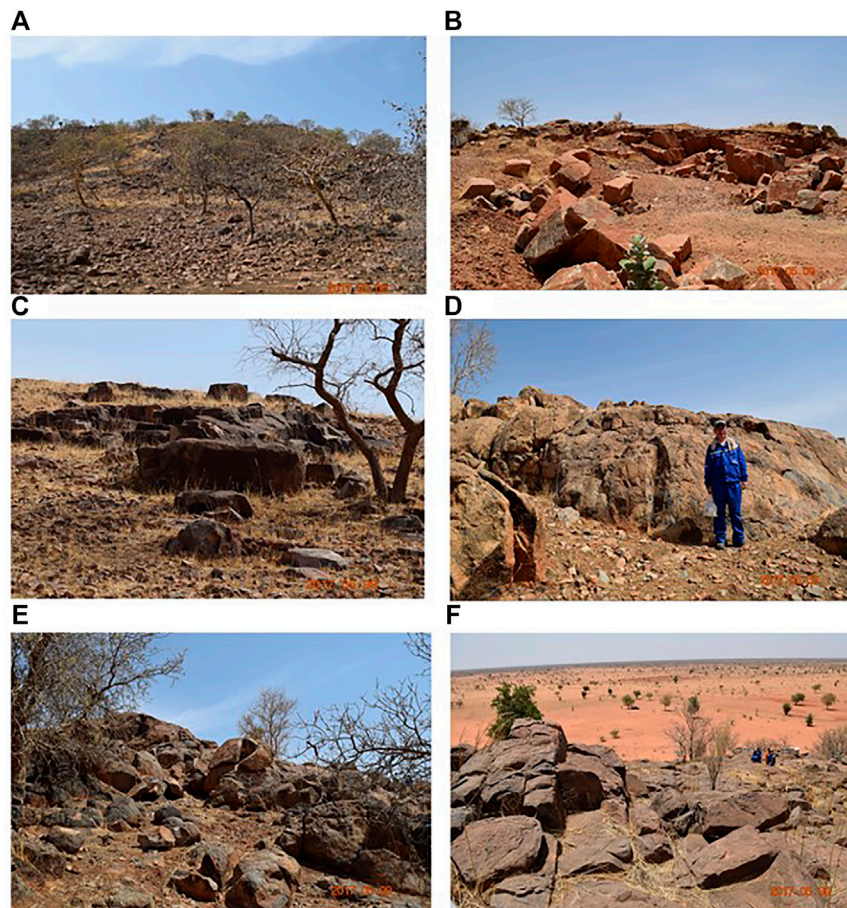
FIGURE 3 | Overview photographs of outcrops. **(A)** Outcrop covered by plant and broken dispersed sandstones (EB -3); **(B)** Outcrop covered by a thin layer of Quaternary loess (UK-5); **(C)** Outcrop partially covered by low shrub (UK-9); **(D)** Outcrop as giant igneous bodies (UK-8); **(E)** Outcrop with dispersed granite bodies (UK-4); **(F)** Outcrops with joints and fractures (UK-4).

All the three sedimentary cycles overly the basement. Up to now, a total of 19 wells have been drilled into the basement in Block-6, with rock penetration thickness ranging from 17 to 257 m. The penetrated intervals are mainly composed of granite or granodiorite that experienced regional metamorphism in different degrees (Zhao et al., 2020).

The studied areas of this work include the East-Baleela-Low-High (EB) in the east margin of Block-6 and the Um-Khashmeen (UK) in the north margin of Block-6, covering nearly 2,700 km^2 (**Figure 2**). They are in a transition zone between the Nuba mountains and the Muglad basin (GRAS, 2005). Due to the uplift of the Nuba Mountain, the strata in the Muglad Basin were tilted towards the mountain, which provided ideal sections and "windows" for basement investigation (**Figure 2**).

MATERIALS AND METHODS

Sample Collection and Description in Field

At least 20 locations were investigated during the whole field trip, of which 15 outcrops (4 in EB area, 11 in UK area) were observed and described in detail (**Figure 2**). For each outcrop, orientation data, as well as photos and some quick sketches, for all the strata, sedimentary structures, fault planes, joints, and fractures were collected. At each outcrop, we sampled different types of rocks and recorded their GPS coordinates, occurrences, and contact relationships with their country rocks.

Laboratory Analysis

About 120 samples were collected in the field and then examined in the laboratory. Samples were named after outcrop and sampling number. For example, EB3-2 is a sample that was collected at the second sampling location at the EB-3 outcrop.

Around 100 thin sections from a total of 80 hand specimens were studied. Petrology and mineralogy were systemically described in terms of rock types, micro-textures, structures, mineral assemblages, mineral species, mineral contents, and mineral alternation.

Zircon geochronology study was conducted on five representative samples from five outcrops, including zircon internal structures, Th and U contents, rare earth elements (REE), and U-Pb dating on more than 200 zircons.

Cathodoluminescence (CL) images were taken on these zircons before analysis to reveal the internal structure and determine the analytical positions. All these obtained data were combined to determine the origin of zircons.

Zircon U-Pb Dating Methods

The single-zircon U-Pb dating method was utilized to estimate the ages of these rocks. Sample preparation and age dating were conducted in the State Key Laboratory of Continental Dynamics at Northwest University, China. The equipment used was a Laser Ablation Inductively Coupled Plasma Mass Spectrometry (LA-ICP-MS) produced by Agilent with a GeoLas200 M laser ablation system produced by MicroLas. The laser ablation system consisted of a Compex102 ArFexcimer laser (operated at a wavelength of 193 nm) from Lambda Physik, with a MicroLas optical system.

Single spot laser ablation was used for sampling, with a spot diameter of 30 μm and a frequency of 10 Hz. The carrier gas for the ablated materials was high-purity argon and helium. Standard zircon 91,500 and synthetic glass NIST610 were used as standards, with one analysis on zircon 91,500 every five spots and one analysis on NIST610 every 10 spots. The background acquisition time for each spot was 30 s and the signal acquisition time was 40 s. GLITTER software (ver. 4.0, Macquarie University) was used for data processing. The zircon standard 91,500 was adopted as the external standard for isotopic ratio fractionation correction during age calculation.

RESULTS

Field Investigations

The outcrops can be roughly divided into two types, covered, and uncovered. The former type of outcrops is usually covered by plants, sparse vegetation (**Figure 3A**), or overlying sedimentary strata such as Quaternary flood deposits (**Figures 3B,C**). Uncovered outcrops have no vegetation cover, and the rocks are completely and directly exposed, appearing as a single giant granite body (**Figure 3D**) or multiple continuous low-amplitude hills (**Figures 3E,F**). Many outcrops have clear broken zones, fractured belts, or joint systems (**Figures 3E,F**).

At least dozens of rock types, either igneous or metamorphic, were identified in the field at different outcrops. The igneous rocks include granite, syenite, diorite, and monzonite and they are relatively fresh (**Figures 4A–C,F**). The metamorphic rocks contain metasandstone, quartzite, gneiss, and mylonite (**Figures 4D,E**). Most outcrops are dominated by igneous rocks (85 vol%), followed by gneiss and quartzite (around 10%), and minor mylonite (less than 5%).

Field Occurrence and Petrology of the Representative UK-7 Outcrop

In this study, the UK-7 outcrop was selected to represent the rock types and their occurrences of the studied outcrops. The rocks at the UK-7 outcrop are directly exposed to the surface (**Figure 5A**) and are typically granite and syenite (**Figure 5A**). Spheroidal weathering is widespread, with hundreds of ball-shaped granites distributed randomly. Fractures often transect veins, joints, and other fractures (**Figures 5A,B**). The rocks are usually flesh red, dense, and massive, with a medium-coarse-grained texture. Aggregates of K- feldspar or hornblende crystals are visible in hand specimens (**Figure 5C**).

Sample UK7-1 is medium-to-coarse-grained syenite, with a subhedral granular texture and grain sizes from 1.0 to 4.0 mm. It is composed of alkali feldspar, plagioclase, and quartz. The dominant alkali feldspar (69%) occurs in both subhedral-tabular and wide-tabular shapes, within which plagioclase commonly appears as metasomatic relics, suggesting intensive alkalization (**Figures 6A,B**). The plagioclase (10%) is tabular, with some polysynthetic twinning. The hornblende (20%), sometimes occurring as aggregates, are subhedral, euhedral granular, and columnar grains, with good cleavages, partial chlorination, and magnetite precipitation. The quartz, with varied contents, is xenomorphic-granular and infilled between tabular feldspar crystals (**Figures 6C,D**). Except for some metasomatic minerals, almost all the mineral crystals are in good shape with sharp boundaries, indicating a weak degree of hydrothermal alteration.

We studied all the collected samples from the 15 outcrops and found that they are more commonly composed of granite, syenite, and diorite, with a minor volume of metasandstone, mylonite, gneiss, and quartzite (**Table 1**). They have similar mineral assemblages of alkali feldspar, plagioclase, quartz, and amphibole (or hornblende). In igneous rocks, alkali feldspar and plagioclase are principal minerals, and their contents could reach as high as 75%. Residual plagioclases are usually developed within alkali feldspar, indicating strong alkalization. The contents of quartz vary from 10% to 25%. And the hornblende is usually with magnetite. These minerals seem fresh without significant alternation, but the micro-fractures and veins are usually developed among them. Metamorphic rocks have various mineral assemblages, and serious mineral alteration. Metasandstone and quartzite are mainly composed of quartz and lithic fragments. Similarly, the mylonite is also composed of the quartz-dominated matrix, showing strong recrystallization and orientation, while gneiss is constituted by biotite, feldspar, and quartz. Most of these minerals are underwent partly to completely alternation (**Table 1**).

Zircon CL Imaging, REE Patterns, and U-Pb Dating Results of Sample UK7-1

Zircon Cathodoluminescence (CL) Characteristics

Cathodoluminescence (CL) imaging is an effective method to reveal the morphology, internal structures of zircons and helps to determine their origin. For example, magmatic zircons typically display oscillatory zoning or fan-shaped zoning structures, while metamorphic zircons have different internal structures, including no zoning, weak zoning, or cloud-like zoning (Wu and Zheng, 2004). Thus, identifying the origin of zircons by CL images could assist to get more geological meaningful ages. CL imaging was conducted on nearly fifty zircons from sample UK7-1. These zircons are large euhedral grains (100–300 μm), with generally

FIGURE 4 | Photographs of different types of rocks from outcrops. **(A)** Alkaline granite pegmatite, with K-feldspar phenocrysts and quartz veins (EB3-5); **(B)** Porphyritic quartz syenite, alkali feldspar phenocrysts (UK 5-1); **(C)** Silicified fine-grained monzonite (UK9-2). **(D)** Altered biotite gneiss, gneissic structure (UK 15-1); **(E)** Mylonite in gray color with high quartz content and certain orientation (UK14-1); **(F)** Fine-grained K-feldspar diorite, with local hornblende aggregates and high content of plagioclase (UK6-1).

strong luminescence showing obvious oscillatory zoning structures (**Figure 7**), indicating their magmatic origin.

Zircon REE Patterns

Zircon grains from sample UK7-1 have low Th (18–509 ppm; mean = 170 ppm) and U contents (40–495 ppm, mean = 186 ppm), with variable Th/U ratios ranging from 0.5 to 1.3, diagnostic of unaltered igneous zircons (Th/U ≥ 0.5) (**Supplementary Appendix S1**). They have relatively high total REE contents (ΣREE = 938–21,853 ppm; mean = 10,758 ppm). The chondrite-normalized REE patterns of zircons from this sample display significant enrichment of heavy REEs relative to light REEs (**Figure 8** and **Supplementary Appendix S2**), with significant positive Ce and negative Eu anomalies, all of which indicate a magmatic origin (Hoskin and Schaltegger, 2003).

Zircon U-Pb Dating of Sample UK7-1

Thirty-six spots were also analyzed on zircons for sample UK7-1 (**Supplementary Appendix S3**). The U-Pb Concordia diagrams suggest that most ages are clustered in a narrow range between 210 Ma and 250 Ma, mainly around 230 Ma. A weighted mean

age of 224 ± 2 Ma was obtained and is a reliable crystallization age of the syenite (**Figure 9**).

Zircon REE Patterns and U-Pb Dating Results of Other Samples

Zircon grains from the sample UK5-2 display low Th (29–131 ppm; mean = 61 ppm) and U contents (76–204 ppm, mean = 131 ppm), with a limited Th/U ratio range of 0.3–0.5 (mean = 0.5). In sample UK6-1, zircons show variable Th (24–4,968 ppm; mean = 939 ppm) and U contents (385–1,460 ppm, mean = 835 ppm), with largely variable Th/U ratios of 0.1–3.4 (mean = 0.9). The Th and U contents of zircon grains from sample UK6-2 are much higher with values of 257–3,281 ppm (mean = 817) and 342–1,688 ppm (mean = 1,076 ppm), respectively. The Th/U ratios of zircons from this sample (mean = 0.8) are mostly higher than 0.5, similar to those of typical igneous zircons. Zircon grains from sample UK11-3 show extremely variable Th (54–5,399 ppm; mean = 1796 ppm) and U contents (106–1,277 ppm; mean = 501 ppm), resulting in largely variable Th/U ratios of 0.5–8.5. All these zircon

FIGURE 5 | Overview of UK-7 outcrop and sampling. **(A)** Overview of the UK-7 outcrop and apparent spheroidal weathering; **(B)** Fractured and spheroidal weathered granite bodies; **(C)** Hand specimen of basement (ID UK7-1) rock for laboratory test. The UTM geographic coordination of sample UK7-1 is X:598492; Y: 1328369.
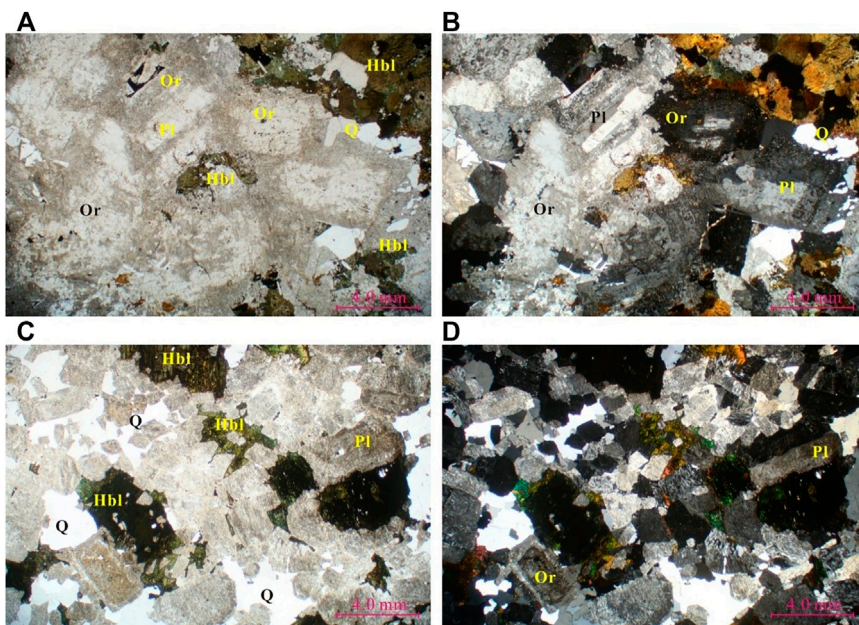

FIGURE 6 | Photomicrographs illustrating the mineral assemblage and typical micro-texture of sample UK7-1. **(A)** Principal minerals, alkali feldspar, plagioclase, and hornblende; **(B)** Wide-tabular alkali feldspar with metasomatized plagioclase; **(C)** Granular, short columnar amphibole with chlorite rims; **(D)** Granular quartz infilled between feldspar and hornblende. Pl, Plagioclase; Or, K-Felspar; Hbl, Hornblende; Q, Quartz.

Th-U data indicate the zircons from these samples are of magmatic origin.

The zircon REE pattern diagrams were also generated. The chondrite-normalized REE patterns of zircons from sample UK5-2 display enrichment of heavy REEs relative to light REEs, with significant positive Ce and negative Eu anomalies (**Figure 10A**). Comparatively, in sample UK6-1, the rising slopes from LREE to HREE are much weaker.

TABLE 1 | Rock types and mineral assemblages of basement rocks in the studied outcrops.

| Rock type	Sub type	Rock name	Micro-texture and micro-structure	Mineral assemblages and typical characteristics	Outcrops and location
Igneous rocks	Granite	Alkaline feldspar granite, granite porphyry, medium-fine-grained alkali feldspar granite, fine-grained hornblende feldspar granite, silicified alkali feldspar granite	Granite structure, porphyritic structure, massive structure	Alkaline feldspar 60%, plagioclase 15%, quartz 25%; phenocrysts are mainly quartz and alkaline feldspar	EB3, UK4, UK5, UK8, UK10
	Syenite	Porphyry quartz syenite, medium-coarse-grained syenite, medium-fine-grained quartz syenite, silicified fine-grain monzonite	Hypidiomorphic-granular texture, porphyritic texture, massive structure	Alkaline feldspar 74%, plagioclase 5%, amphibole 7%, magnetite 4%, quartz 10%. Residual plagioclase in alkaline feldspar indicates strong alkalization	UK4, UK5, UK6, UK7,UK9
	Diorite	Fine-grained diorite, fine-grained quartz diorite	Hypidiomorphic-granular texture, massive structure	Plagioclase 57%, hornblende 43% (precipitating magnetite), or plagioclase 50%, hornblende 37%, quartz 13%	UK6
Metamorphic rocks	Metamorphic sandstone	Coarse-grained metamorphic conglomerate sandstone, metamorphic fine-grained quartz sandstone	palimpsest texture, massive structure, local quartzite	Quartz 60%, lithic fragment 40%	EB3, UK11
	Mylonites	Mylonite	Mylonitic structure, ocellar structure	composed of fragments and groundmass, fragments 10%, eyeball-like distribution, completely altered to clay; the quartz groundmass underwent strong recrystallization, oriented and in striped distribution	UK14
	Gneiss	Altered biotite gneiss	lepidoblastic texture, gneiss structure	biotite 30%, altered feldspar 30%, quartz 30%	UK15
	Quartzite	Quartzite, silicified rock	Coarse-large-grained crystalloblastic texture, massive structure	Mainly composed of quartz, with undulose extinction	UK16, UK11
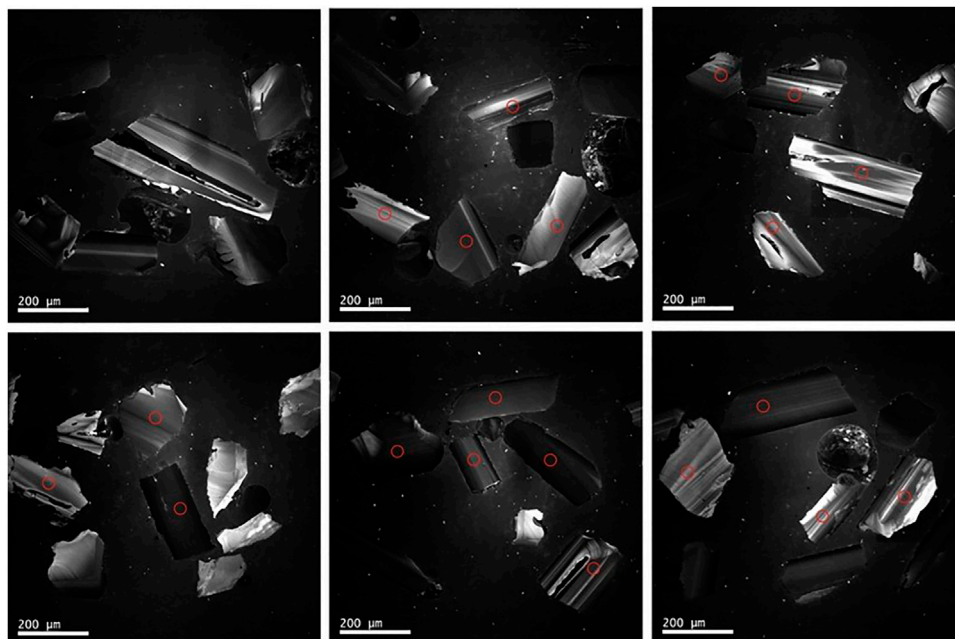
FIGURE 7 | CL images of zircons from sample UK7-1. CL images show strong luminance with obvious oscillatory zoning structures. (Red circles representing analytical points).
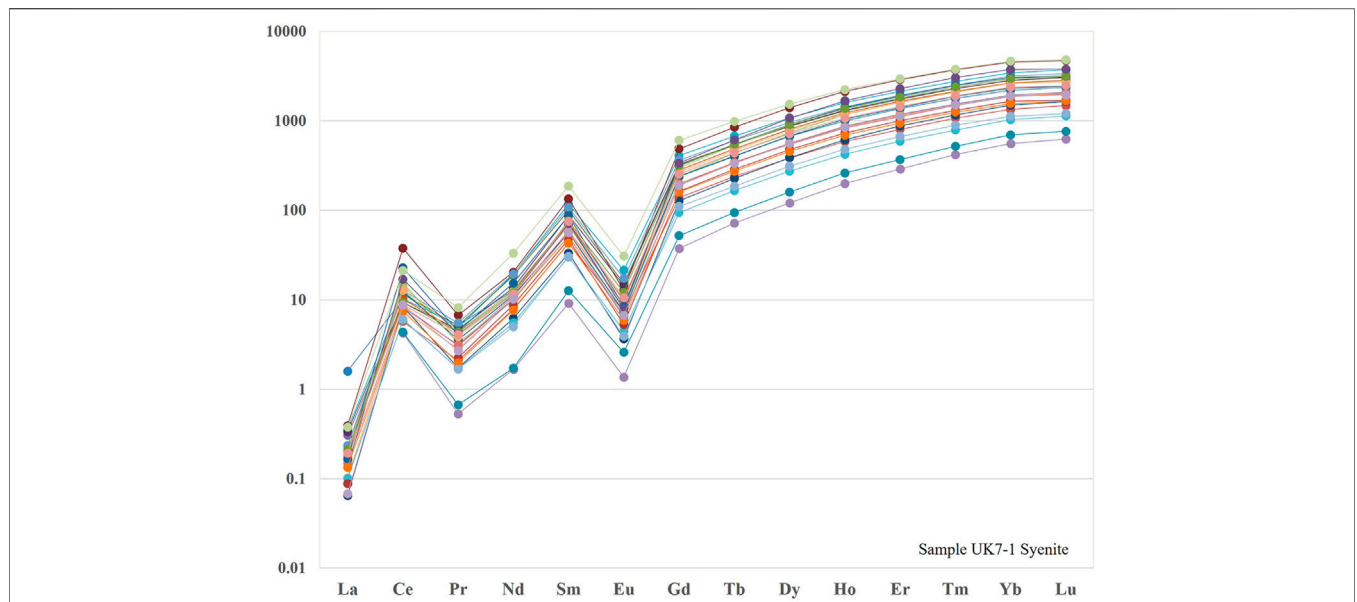
FIGURE 8 | REE distribution pattern of zircons of sample UK7-1. Enrichment of heavy REEs relative to light REEs, with significant positive Ce and negative Eu anomalies.
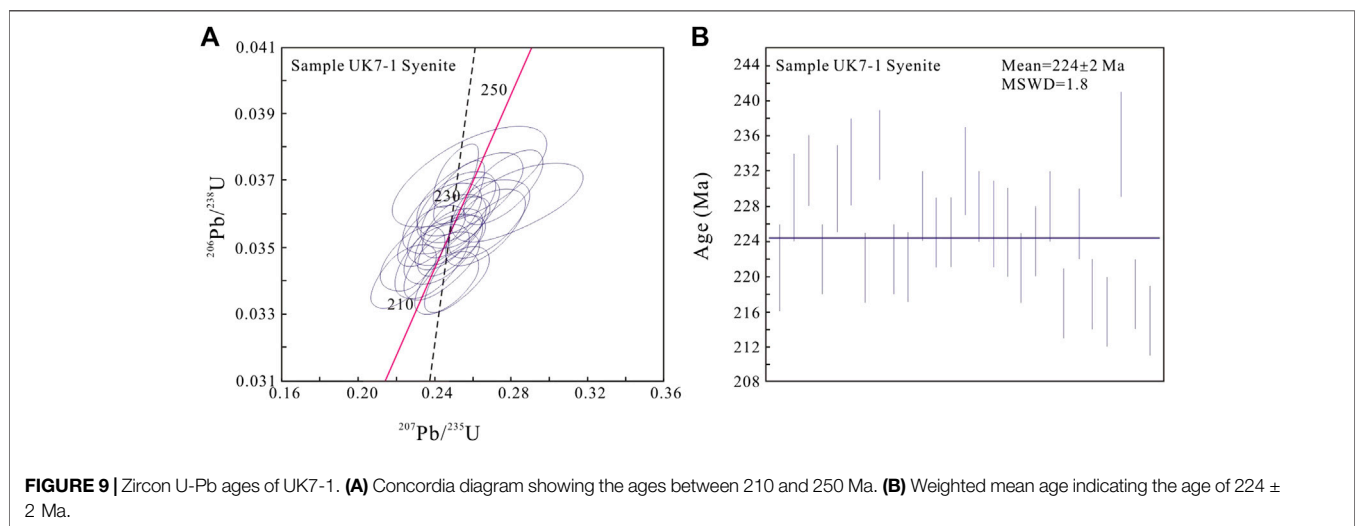

FIGURE 9 | Zircon U-Pb ages of UK7-1. **(A)** Concordia diagram showing the ages between 210 and 250 Ma. **(B)** Weighted mean age indicating the age of 224 ± 2 Ma.
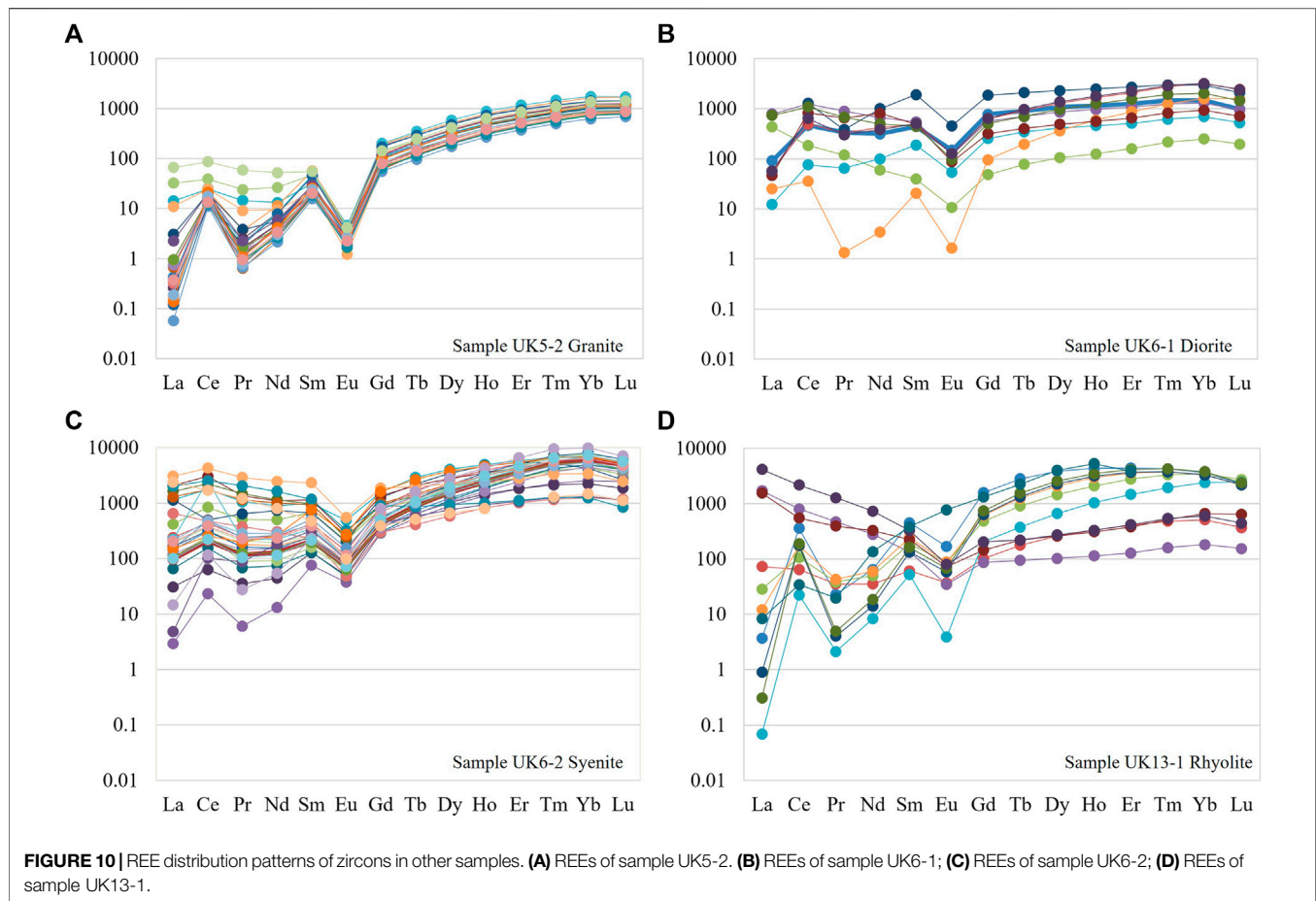
However, the positive Ce and negative Eu anomalies remain obvious (**Figure 10B**). For sample UK 6-2, the zircons also display a steeply rising slope but relatively weak positive Ce anomalies and negative Eu anomalies among other samples (**Figure 10C**). Sample UK 11-3 also show significant positive Ce and negative Eu anomalies (**Figure 10D**). All these characteristics of zircon trace elements indicate the zircons are of magmatic origin (Hoskin and Schaltegger, 2003).

Using the same dating method and following the same procedure as those of sample UK7-1, we tested another 144 individual zircon grains from samples UK5-2, UK 6-1, UK6-2, and UK11-3. The sample ages were obtained either from the Concordia graph,

weighted mean age, or both. Sample UK5-2 has a Concordia age of 217.8 ± 1.7 Ma, consistent with the weighted mean age of 218 ± 2 Ma (**Figures 11A,B**). The Concordia diagram of UK 6-1 revealed an age of 224.8 ± 3 Ma (**Figure 11C**), while the sample UK6-2 shows an intercept age at 207.2 ± 5.9 Ma (**Figure 11D**). The ages from sample UK 11-3 are a little dispersed and give a mean age of 195 ± 6 Ma (**Figures 11E,F**). All these ages were summarized in **Table 2**.

DISCUSSIONS

Based on the mineral assemblage, zircon CL imaging, and U-Pb dating data, we speculate that most outcrops are mainly composed of

FIGURE 10 | REE distribution patterns of zircons in other samples. **(A)** REEs of sample UK5-2. **(B)** REEs of sample UK6-1; **(C)** REEs of sample UK6-2; **(D)** REEs of sample UK13-1.

granite and granodiorite, with similar mineral associations, micro-textures, and structures. The zircon oscillatory zoning, the Th/U ratios, and REE patterns all indicate their magmatic origin.

The obtained U-Pb ages are reliable and robust, revealing these rocks were formed in Late Triassic-Early Jurassic. For the first time, the Late Triassic-Early Jurassic magmatic events have been identified in the basement of the Muglad Basin area and the whole CARS.
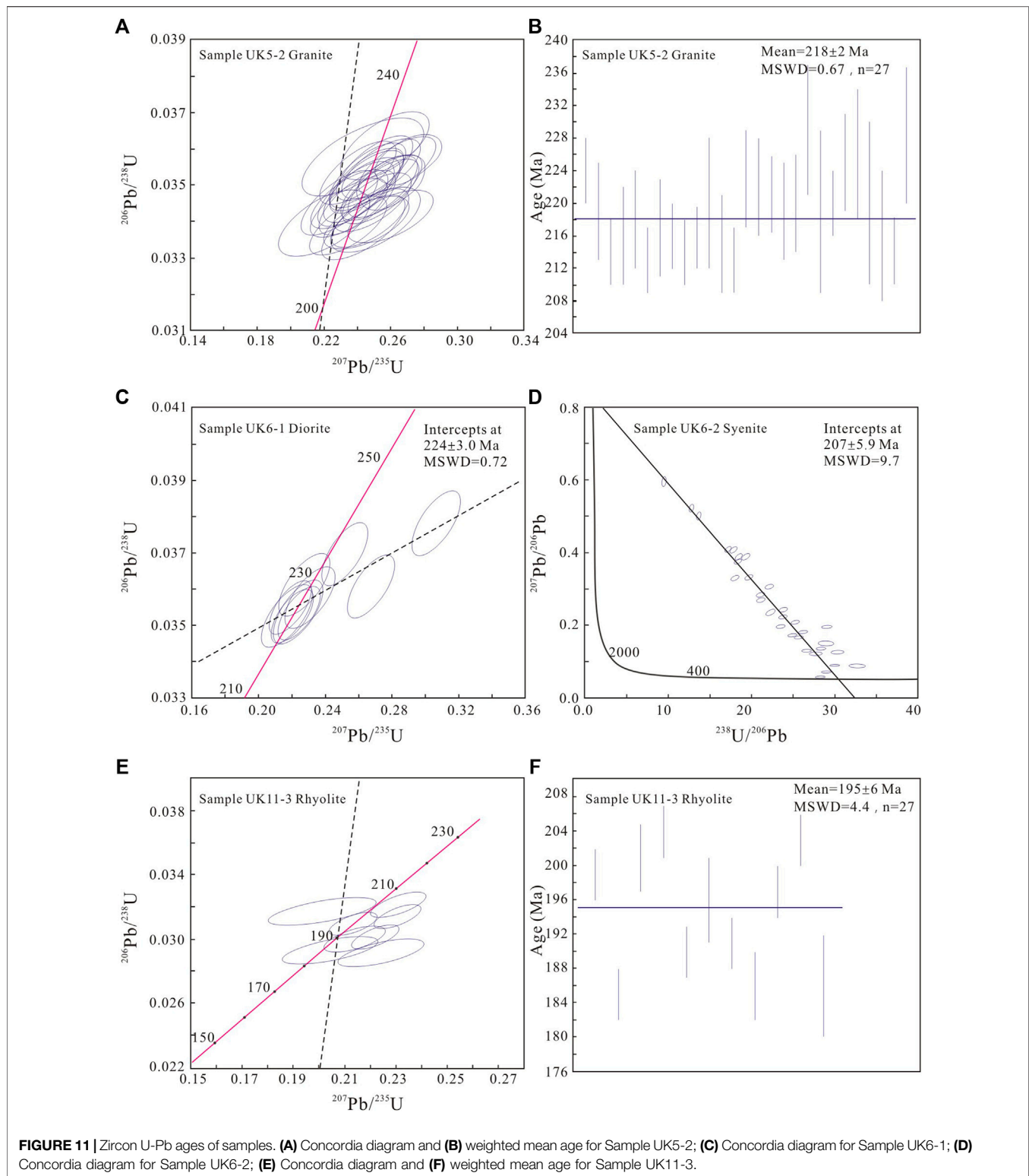
New Member of the Basement of the Muglad Basin

Before the basin-rifting stage, from Precambrian to Late Jurassic, the CARS rarely experienced large-scale intraplate magmatic events, so the Precambrian granite intrusions are very limited in the basin basement. However, since the beginning of basin-rifting in the Cretaceous, the CARS have undergone frequent and intensive magmatic events due to intraplate extension. At least three regional magmatic events took place, i.e., the Early Cretaceous (147–106 Ma), Late Cretaceous (95–75 Ma), and Paleogene (66–52 Ma) events. The main igneous rocks are basalt and diorite, and they are common in the Bongor, Termit, and Doba Basins (**Table 3**; Wilson et al., 1992; Guiraud and Maurin, 1992; Guiraud et al., 1992; Janssen et al., 1995; Maluski et al., 1995; Coulon et al., 1996; Kamdem et al., 2002; Lu et al., 2009).

The identification of the Late Triassic-Early Jurassic intrusions in addition to the Later Cretaceous intrusions indicates that some local thermal or magmatic events also occurred in the Early Mesozoic. These intrusions resulted in changes in rock association and basement morphology. These Early Mesozoic intrusions are therefore a new member to the basement of the Muglad Basin in addition to the Precambrian rocks.

A New Candidate for Basement Reservoir

As mentioned above, the lithology of the basement has fundamental impacts on the development of an unconventional reservoir (Hu et al., 1981; Dou et al., 2015; 2018). The primary minerals of the Late Triassic-Early Jurassic igneous rock in the Muglad Basin are feldspars (both potassic and plagioclase) and quartz, with various amounts of dark minerals (mainly hornblende and biotite). These mineralogical compositions of felsic rocks with inherent susceptibility to alteration and diagenesis makes them better candidates for basement reservoirs. Adjacent to these outcrops, drilled wells and three-dimension seismic data (3D seismic) in Block-6 have revealed a double-layer structure for the basement. The shallow layer is the weathered crust, and the middle-deep layer is mainly fractured zones (Zhao et al., 2020). The crust is mainly constituted by these granitoids and has very good porosity and permeability. Its thickness varies from area to area and is

FIGURE 11 | Zircon U-Pb ages of samples. **(A)** Concordia diagram and **(B)** weighted mean age for Sample UK5-2; **(C)** Concordia diagram for Sample UK6-1; **(D)** Concordia diagram for Sample UK6-2; **(E)** Concordia diagram and **(F)** weighted mean age for Sample UK11-3.

usually less than 50 m (Zhao et al., 2020). Similarly, in the Bongor basin (Chad), the thickness of the weathered crust could reach up to hundreds of meters with excellent porosity and permeability, and they are also the product of granitic basement weathering (Dou et al., 2015; 2018; Dou et al., 2018).

In addition, these intrusive rocks were formed as early as in the Early Mesozoic. After that, they experienced regional uplifting, mechanical breaking, physical weathering, and leaching for as long as 65 Ma – 95 Ma during and after the basin formation. This long-time duration of weathering and leaching would

TABLE 2 | Summary of LA-ICP-MS U-Pb zircon ages of all samples.

Sample	Sample ID	Lithology	Age	Stage
1	UK5-2	porphyritic alkali feldspar granite	218 ± 2 Ma	Norian of Triassic
2	UK6-1	fine grained k-feldspar quartz diorite	225 ± 3 Ma	
3	UK6-2	fine-grained quartz syenite	207 ± 5 Ma	Rhaetian of Triassic
4	UK11-3	rhyolite (creolite)	195 ± 6 Ma	Sinemurian of Jurassic
5	UK7-1	medium-coarse syenite	224 ± 2 Ma	Norian of Triassic

TABLE 3 | Magmatic events and geochronology in the basins across the CARS (After Dou et al., 2018).

Basin	Well	Depth/m	Occurrence and location	K-Ar Age/Ma	Geological chronology
Bongor	Ronier-1	1895–1900	Intrusive rock in lower Cretaceous	65.6 ± 2.4	Paleogene
		1950–1955	Intrusive rock in lower Cretaceous	65.3 ± 3.1	Paleogene
		1980–1985	Intrusive rock in lower Cretaceous	59.6 ± 2.1	Paleogene
Termit	Acacia-1	1,490–1,495	Intrusive rock in upper Cretaceous	63.1 ± 2.2	Paleogene
		1,550–1,555	Intrusive rock in upper Cretaceous	62.8 ± 1.8	Paleogene
Doba	Nere-1	940–945	Intrusive rock in upper Cretaceous	79.0 ± 2.3	Later Cretaceous
		1,625–1,630	Intrusive rock in lower Cretaceous	93.5 ± 2.9	Later Cretaceous
	Figuier-1	50–60	Intrusive rock in upper Cretaceous/partly exposed basement	95.0 ± 2.0	Later Cretaceous
		1,680–1,685	Intrusive rock in lower Cretaceous	88.4 ± 2.5	Later Cretaceous

significantly improve their porous and permeable properties and form weathering-leaching zone or fissures-fracture zone of considerable scale and thickness. The exploration practice in the Bongor basin (Chad) revealed that the weathered crust in high buried hills is much thicker than that in low buried hills. This is mainly because the weathering time of high buried hills is longer than that of low buried hills before they were buried, indicating the impact of weathering time on basement reservoir development (Dou et al., 2018).

Finally, the outcrops are adjacent to the CARS, with strong tectonic activities and frequent changes in the tectonic stress regime, which provide external conditions for the formation of fractures and the improvement of reservoir properties (Genik, 1992; Fairhead et al., 2013). The geological field investigations found multi-stage fractures in these outcrops. Meanwhile, millimeter-sized fractures can also be seen in thin sections (Zhao et al., 2020).

Further Research on the Mesozoic Intrusions

Although the Mesozoic intrusions are first discovered and reported in this study, we do not know their regional distribution due to the limited study area compared to the Muglad Basin. Based on our field investigation and laboratory analysis, we intend to believe that these intrusive bodies are sills exposed at these outcrops. They may come from the same magma chamber in deep layer because they all share similar mineral assemblages, ages, and chemical compositions. It is anticipated that these intrusions may be developed in a much larger area, and more and more discoveries will be made in the future. To clarify their types and scales, additional geological surveys and geophysical work should be conducted in the future. Then their representativeness should be further demonstrated across the basin.

Besides, magmatism and its implication for tectonic evolution would be one major part of the next-stage research. Because magmatism is probably related to regional rifting. The volcanic activities in Chad basins were reported as the products of the intraplate extensional stress regime, corresponding to the tectonic setting of the whole West and the Central during the Cretaceous (Lu et al., 2009). A comprehensive study of these topics will help understand the scientific significance of this episode of magmatism and shed light on future regional geological surveys and oil and gas exploration.

CONCLUSIONS

The Late Triassic-Early Jurassic rocks in the Muglad Basin are mainly intermediate-acid intrusive rocks, including granite, syenite, diorite, and monzonite, with principal minerals of alkali feldspar, plagioclase, quartz, and minor hornblende, biotite, and magnetite. The oscillatory zoning in CL images, Th/U ratios, and REE patterns of zircons from these intrusions indicate their magmatic origin. These intrusions have zircon U-Pb ages ranging from 195.0 ± 6 to 225.0 ± 3 Ma.

For the first time, the Late Triassic-Early Jurassic intrusive rocks were identified in the CARS region, indicating that the old basement was subjected to younger magmatic intrusion. Therefore, the Muglad Basin consists of at least two major generations of basement rocks: Precambrian rocks and Early Mesozoic intrusions, and thus the basement in the CARS is unlikely a "uniform craton" as traditionally considered.

Together with the Precambrian basement, the Early Mesozoic igneous rocks experienced at least 65–95 Ma of weathering and fracturing during the formation and evolution of the Muglad basin, which may have formed an unconventional reservoir. As a new target for hydrocarbon exploration, the potential of the

basement in the Muglad Basin and the whole CARS is probably underestimated.

DATA AVAILABILITY STATEMENT

The original datasets presented in the study are included in the article/**Supplementary Material**, further inquiries can be directed to the corresponding author.

AUTHOR CONTRIBUTIONS

JZ, conducted the field trip and collected the samples for laboratory tests and analysis. LR-D, fully in charge of this comprehensive research project, providing academic guidance and technical supervision.

FUNDING

ACKNOWLEDGMENTS

SUPPLEMENTARY MATERIAL

The Supplementary Material for this article can be found online at: https://www.frontiersin.org/articles/10.3389/feart.2022.853082/full#supplementary-material

REFERENCES

Awad, M. Z. (2015). *Petroleum Geology and Resource of Sudan*. Berlin: Geozon Science Dedia UG, 427.

Binks, R. M., and Fairhead, J. D. (1992). A plate tectonic setting for the Mesozoic rifts of Western and Central Africa, in P. A. Ziegler, ed., Geodynamics of rifting, volume II. Case history studies on rifts, North and South America: Tectonophysics: Amsterdam, Elsevier. 213, 141–151. doi:10.1016/0040-1951(92)90255-5

Coulon, C., Vidal, P., Dupuy, C., Baudin, P., Popoff, M., Maluski, H., et al. (1996). The Mesozoic to Early Cenozoic Magmatism of the Benue Trough (Nigeria); Geochemical Evidence for the Involvement of St Helena Plume. *J. Petrol.* 37 (6), 1364–1358. doi:10.1093/petrology/37.6.1341

Dou, L. R., Wei, X. D., Wang, J. C., Li, J. L., Wang, R. C., and Zhang, S. H. (2015). Characteristics of Granitic Basement Reservoir in Bongor Basin (In Chinese with English Abstract). *Acta Petrolei Sinica* 36 (8), 898–903. doi:10.7623/syxb201508001

Dou, L. R., Xiao, K. Y., and Wang, J. C. (2018). *Petroleum Geology and Exploration Practice in Intensive Inversion Rift basin (In Chinese)*. Beijing, China: Petroleum Industry Press.

Dou, L. R., Wang, J. D., Wang, R., Wei, X., and Shrivastava, C. (2018). Precambrian Basement Reservoirs: Case Study from the Northern Bongor Basin, the Republic of Chad. *AAPG Bull.* 102 (9), 1803–1824. doi:10.1306/02061817090

Fairhead, J. D., Green, C. M., Masterton, S. M., and Guiraud, R. (2013). The Role that Plate Tectonics, Inferred Stress Changes and Stratigraphic Unconformities Have on the Evolution of the West and Central African Rift System and the Atlantic continental Margins. *Tectonophysics* 594, 118–127. doi:10.1016/j.tecto.2013.03.021

Fairhead, J. D. (1988b). "Late Mesozoic Rifting in Africa," in *Triassic-Jurassic Rifting, continental Breakup and the Origin of the Atlantic Ocean and Passive Margins*. Editor W. Manspeizer (New York: Elsevier), 998. doi:10.1016/b978-0-444-42903-2.50038-5

Fairhead, J. D. (1988a). Mesozoic Plate Tectonic Reconstructions of the central South Atlantic Ocean: The Role of the West and Central African Rift System. *Tectonophysics* 155, 181–191. doi:10.1016/0040-1951(88)90265-x

Fairhead, J. D. (1992). The West and Central African Rift Systems: Foreword. *Tectonophysics* 213 (1-2), 139–140. doi:10.1016/b978-0-444-89912-5.50033-8

Genik, G. J. (1993). Petroleum Geology of Cretaceous-Tertiary Rift Basins in Niger, Chad and the Central African Republic [J]. *AAPG Bull.* 77 (8), 1405–1434. doi:10.1306/bdff8eac-1718-11d7-8645000102c1865d

Genik, G. J. (1992). Regional Framework, Structural and Petroleum Aspects of Rift Basins in Niger, Chad and the Central African Republic (C.A.R.). *Tectonophysics* 213 (1/2), 169–185. doi:10.1016/b978-0-444-89912-5.50036-3

GRAS (2005). *Geological Map of the Sudan, Scale 1*. Sudan: Ministry of Energy & Mines, Geological & Mineral Resources Department, Khartoum, 20000000. [M].

Guiraud, R., Binks, R. M., Fairhead, J. D., and Wilson, M. (1992). Chronology and Geodynamic Setting of Cretaceous-Cenozoic Rifting in West and Central Africa. *Tectonophysics* 213, 227–234. doi:10.1016/0040-1951(92)90260-d

Guiraud, R., and Maurin, J.-C. (1992). Early Cretaceous Rifts of Western and Central Africa: an Overview. *Tectonophysics* 213 (1-2), 153–168. doi:10.1016/b978-0-444-89912-5.50035-1

Hoskin, P. W. O., and Schaltegger, U. (2003). 2. The Composition of Zircon and Igneous and Metamorphic Petrogenesis. *Rev. mineralogy Geochem.* 53 (1), 27–62. doi:10.1515/9781501509322-005

Hu, J. Y., Tong, X. G., and Xu, S. B. (1981). Regional Distribution of Buried-hill Reservoirs in Bohai Bay Basin, China (In Chinese with English Abstract). *Pet. exploration Dev.* 5, 1–9.

Janssen, M. E., Stephenson, R. A., and Cloethingh, S. (1995). Temporal and Spatial Correlations between Changes in Plate Motions and the Evolution of Rifted Basins in Africa. *Geol. Soc. Am. Bull.* 107 (11), 1217–1322. doi:10.1130/0016-7606(1995)107<1317:tascbc>2.3.co;2

Kamdem, J. B., Kraml, M., Keller, J., and Henjes-Kunst, F. (2002). Cameroon Line Magmatism: Conventional K/Ar and Single-crystal Laser Ages of Rocks and Minerals from the Hossere Nigo Anorogenic Complex, Cameroon. *J. Afr. Earth Sci.* 35, 99–105. doi:10.1016/s0899-5362(02)00002-7

Li, W., Dou, L. R., Wen, Z. G., Zhang, G. Y., Cheng, D. S., Du, Y. B., et al. (2017). Buried-hill Hydrocarbon Genesis and Accumulation Process in Bongor Basin, Chad (In Chinese with English Abstract). *Acta Petrolei Sinica* 38 (11), 1253–1262. doi:10.7623/syxb201711004

Lu, Y., Liu, J., Lirong, D., Guo, Z., Xiao, K., Hu, Y., et al. (2009). K-ar and 39 Ar-40 Ar Geochronology of Basalts from the Chad Basin, Africa and its Geodynamics Setting (In Chinese with English Abstract). *Acta Geologica Sinica* 83 (8), 1125–1133.

Maluski, H., Coulon, C., Popoff, M., and Baudin, P. (1995). 40Ar/39Ar Chronology, Petrology and Geodynamic Setting of Mesozoic to Early Cenozoic Magmatism from the Benue Trough, Nigeria. *J. Geol. Soc.* 152, 311–326. London. doi:10.1144/gsjgs.152.2.0311

McHargue, T. R., Heidrick, T. L., and Livingston, J. E. (1992). Tectonostratigraphic Development of the Interior Sudan Rifts, Central Africa. *Cent. Africa: Tectonophysics* 213 (1–2), 187–202. doi:10.1016/b978-0-444-89912-5.50037-5

Penaye, J., Kröner, A., Toteu, S. F., Van Schmus, W. R., and Doumnang, J.-C. (2006). Evolution of the Mayo Kebbi Region as Revealed by Zircon Dating: An Early (Ca. 740Ma) Pan-African Magmatic Arc in Southwestern Chad. *J. Afr. Earth Sci.* 44, 530–542. doi:10.1016/j.jafrearsci.2005.11.018

Schandelmeier, H., and Pudlo, D. (1990). The Central African Fault Zone (CAFZ) in Sudan-a Possible continental Transform Fault. *Berl Geowiss Abh A* 120 (1), 31–44.

Schull, T. J. (1988). Rift Basins of interior Sudan: Petroleum Exploration and Discovery. *AAPG Bull.* 72 (10), 1128–1142. doi:10.1306/703c9965-1707-11d7-8645000102c1865d

Tong, X.-G., Lirong, D., Tian, Z.-J., Pan, X.-H., and Zhu, X.-D. (2004). Geological Mode and Hydrocarbon Accumulating Mode in Muglad Passive Rift basin, Sudan (In Chinese with English Abstract). *Acta Petrolei Sinica* 25 (1), 19–24.

Vail, J. R. (1972). Pre-Nubian Tectonic Trends in Northeastern Sudan. *J. Geol. Soc.* 128, 21–31. doi:10.1144/gsjgs.128.1.0021

Wilson, M., Guiraud, R., and Guiraud, R. (1992). Magmatism and Rifting in Western and Central Africa, from Late Jurassic to Recent Times. *Tectonophysics* 213 (1-2), 203–225. doi:10.1016/b978-0-444-89912-5.50038-7

Wu, Y. B., and Zheng, Y. F. (2004). Mineralogy of Zircon and its Constraints on the Interpretation of U-Pb Age (In Chinese with English Abstract). *China Acad. J.* 49 (16), 1589–1604. doi:10.1007/bf03184122

Yassin, M. A., Hariri, M. M., Abdullatif, O. M., Korvin, G., and Makkawi, M. (2017). Evolution History of Transtensional Pull-Apart, Oblique Rift basin and its Implication on Hydrocarbon Exploration: A Case Study from Sufyan Sub-basin, Muglad Basin, Sudan. *Mar. Pet. Geology.* 79, 282–299. doi:10.1016/j.marpetgeo.2016.10.016

Zhao, J., Zhang, G., Liu, A., Ke, W., Shi, Y., Zou, Q., et al. (2020). Development Characteristics and Exploration Significance of Basement Reservoirs in Block-6 of the Muglad Basin, Sudan (In Chinese with English Abstract). *China Pet. exploration* 25 (4), 133–142. doi:10.3969/j.issn.1672-7703.2020.04.014